

MINER: Multiscale Implicit Neural Representations

VISHWANATH SARAGADAM, JASPER TAN, GUHA BALAKRISHNAN,
RICHARD G. BARANIUK, ASHOK VEERARAGHAVAN, ECE Department, Rice University, USA

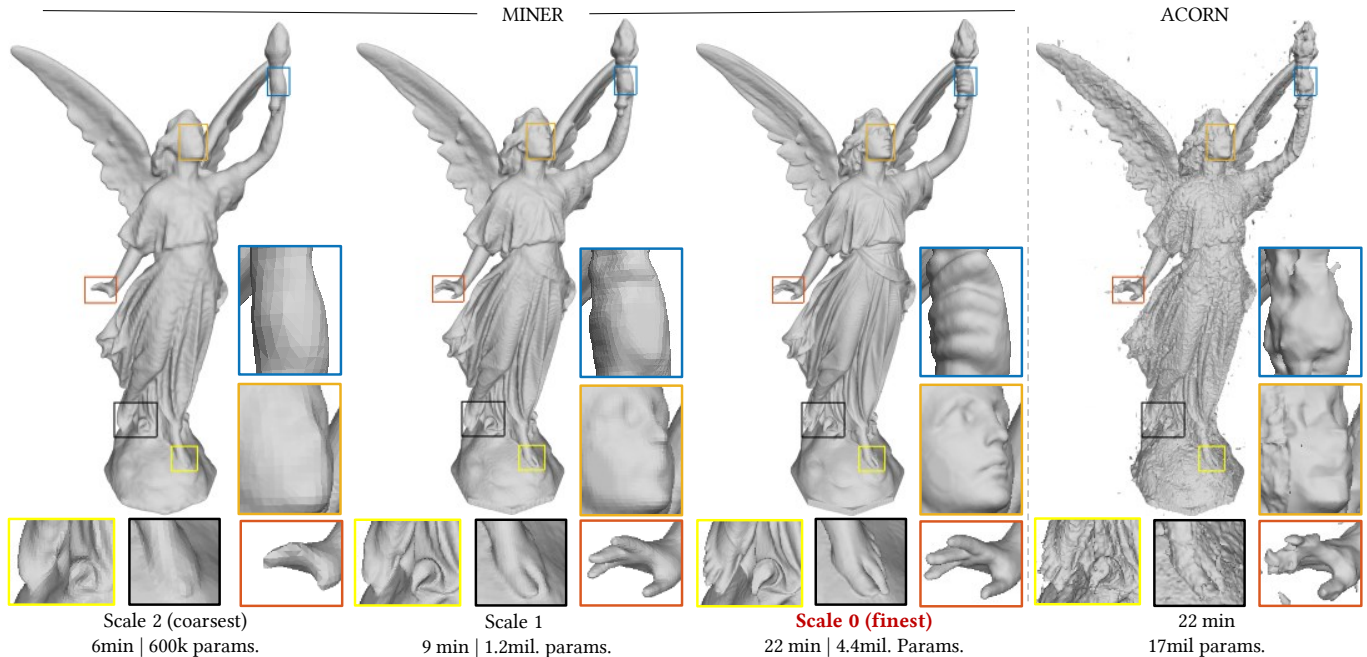


Fig. 1. **Multiscale Implicit Representations.** We present a novel implicit representation framework called MINER that is well suited for very large visual signals such as images, videos, and 3D volumes. We leverage the self-similarity of visual signals across scales to iteratively represent models from coarse to fine scales, resulting in a dramatic decrease in inference and training time, while requiring fewer parameters and less memory than state-of-the-art representations. This figure demonstrates fitting of the Lucy 3D mesh over four scales with scale 3 being the coarsest and 0 being the finest. MINER achieves high quality results across all scales with high IoU value and achieves an IoU of 0.999 at the finest scale in less than 30 minutes. In comparison, the state-of-the-art approach (ACORN) results in an IoU of 0.97 in that time, while requiring far more parameters.

We introduce a new neural signal representation designed for the efficient high-resolution representation of large-scale signals. The key innovation in our *multiscale implicit neural representation* (MINER) is an internal representation via a Laplacian pyramid, which provides a sparse multiscale representation of the signal that captures orthogonal parts of the signal across scales. We leverage the advantages of the Laplacian pyramid by representing small disjoint patches of the pyramid at each scale with a tiny MLP. This enables the capacity of the network to adaptively increase from coarse to fine scales, and only represent parts of the signal with strong signal energy. The parameters of each MLP are optimized from coarse-to-fine scale

which results in faster approximations at coarser scales, thereby ultimately an extremely fast training process. We apply MINER to a range of large-scale signal representation tasks, including gigapixel images and very large point clouds, and demonstrate that it requires fewer than 25% of the parameters, 33% of the memory footprint, and 10% of the computation time of competing techniques such as ACORN to reach the same representation error.

CCS Concepts: • **Computing methodologies** → **Neural networks; Hierarchical representations.**

Additional Key Words and Phrases: neural representations, Laplacian pyramids

ACM Reference Format:

Vishwanath Saragadam, Jasper Tan, Guha Balakrishnan, Richard G. Baraniuk, Ashok Veeraraghavan. 2022. MINER: Multiscale Implicit Neural Representations. *ACM Trans. Graph.* 37, 4, Article 111 (January 2022), 12 pages. <https://doi.org/10.1145/1122445.1122456>

1 INTRODUCTION

The bedrock of modern signal processing is a concise signal representation that can then be utilized for all manner of applications from compression to inverse estimation. Neural implicit representations offer such a concise way to represent discrete data as samples

Author's address: Vishwanath Saragadam, Jasper Tan, Guha Balakrishnan, Richard G. Baraniuk, Ashok Veeraraghavan, ECE Department, Rice University, Houston, USA, vishwanath.saragadam@rice.edu.

Permission to make digital or hard copies of all or part of this work for personal or classroom use is granted without fee provided that copies are not made or distributed for profit or commercial advantage and that copies bear this notice and the full citation on the first page. Copyrights for components of this work owned by others than ACM must be honored. Abstracting with credit is permitted. To copy otherwise, or republish, to post on servers or to redistribute to lists, requires prior specific permission and/or a fee. Request permissions from permissions@acm.org.

© 2022 Association for Computing Machinery.

0730-0301/2022/1-ART111 \$15.00

<https://doi.org/10.1145/1122445.1122456>

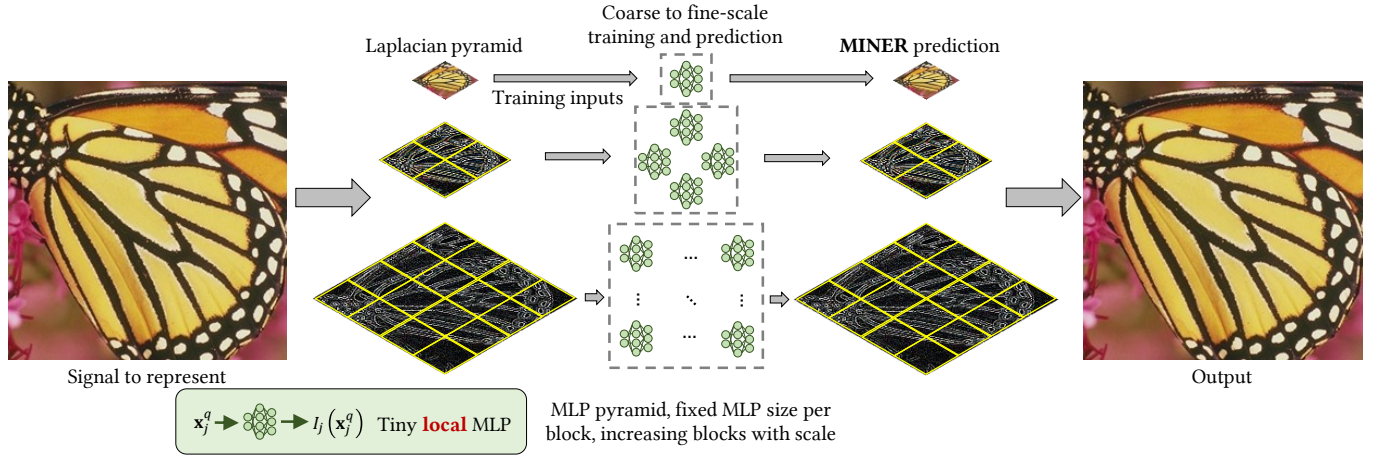


Fig. 2. **MINER trains and predicts Laplacian pyramids.** Visual signals are similar across scales and are compactly represented by Laplacian pyramids. MINER follows a similar scheme where each scale of the Laplacian pyramid is represented by multiple, local MLPs with a small number of parameters. The number of such MLPs increase by a factor of 2 from coarse to fine scale, thereby representing a fixed spatial size at each scale. This multi-scale representation naturally lends itself to a sequential, coarse-to-fine scale training process that is fast and memory efficient.

of a continuous manifold. This enables an efficient way to interpolate data between samples and has found numerous applications in 3D representations [Kuznetsov et al. 2021; Mildenhall et al. 2020; Peng et al. 2020; Srinivasan et al. 2021], images [Chen et al. 2021b], video [Chen et al. 2021a], and linear inverse problems [Chen et al. 2021b; Sun et al. 2021].

Despite their numerous advantages, neural representations suffer from high computational complexity, large memory footprint while training, and a large number of parameters to achieve high accuracy. While there have been several modifications to the network architecture [Martel et al. 2021; Reiser et al. 2021; Sitzmann et al. 2020] and inference [Yu et al. 2021], the existing approaches are not practical for very large signals such as multi-gigapixel images, or 3D point clouds with billions of data points.

We introduce Multiscale Implicit Neural Representations (MINER) that predicts a Laplacian pyramid at multiple spatial scales. Our key observation is that a Laplacian pyramid offers a sparse and multi-scale decomposition that separates different frequency content of the signal into different bands [Adelson et al. 1984; Do and Vetterli 2003], meaning that signals at different bands are approximately orthogonal to one another. We leverage this observation by training MLPs to predict the signal at the coarsest scale and residues at finer scales, achieving a compact representation. A single global MLP at each scale is however ill-suited to leverage the sparseness of the Laplacian transform of visual signals. MINER instead represents local 2D and 3D patches of images and videos with small MLPs, which is similar in structure to recently proposed KiloNeRF [Reiser et al. 2021] representation. The multi-patch decomposition is performed at every scale, with the number of spatial or volume blocks doubling along each dimension as we go from coarse to fine scale. MINER offers a fast and flexible multi-resolution inference, as computing the signal value at lower resolution requires evaluation of fewer MLPs. An overview of MINER is presented in Fig. 2.

The multiscale, multi-MLP architecture is well-suited for fast and memory-efficient training procedure. At each spatial scale, the parameters of the MLPs are trained for the downsampled version of the signal at that scale. We then *sequentially* train MLPs from coarsest scale to the finest scale. To leverage correlations across scales during the training phase, we propose two innovations. First, we demonstrate that training on a Laplacian pyramid (composed of difference signals) is significantly faster than training on a Gaussian pyramid (composed of downsampled signals) as MLPs at finer scales represent information orthogonal to the representation at coarser scales. Second, we compare the upsampled signal from the fine block and target signal at fine block – if the error in representation is smaller than a threshold, we prune out the blocks before training starts. Since visual signals are sparse in their Laplace transform, the fitting converges for parent blocks at a coarser scale, leading to fewer blocks to train at subsequent resolutions. These two modifications result in a dramatic increase in training speed without compromising on memory requirements or total number of parameters. As a result, MINER is 10× or more faster compared to state-of-the-art implicit representations in terms of training process for a comparable number of parameters and target accuracy. MINER can represent gigapixel images with greater than 38dB accuracy in less than three hours, compared to more than a day with techniques such as ACORN [Martel et al. 2021]. For 3D point clouds, MINER achieves an intersection over union (IoU) of 0.999 or higher in less than three minutes, resulting in two orders of magnitude speed up over ACORN. Figure 1 shows results obtained by MINER at the end of training at each spatial scale, along with result from ACORN for the same training time – showcasing how MINER achieves high quality results gradually from low resolution to high resolution.

MINER combines the compact multiscale representations offered by Laplacian pyramids along with the advantages of implicit representations. Due to the multiscale representation, MINER can be used for streaming reconstruction of images, as with JPEG2000 [Shapiro

2009], or efficiently sampling for rendering purposes with octrees [Yu et al. 2021] – making neural representations ready for extremely large scale visual signals.

2 PRIOR WORK

MINER draws inspiration from classical multiscale techniques and more recent neural representations. We outline some of the salient works here to set context.

Implicit neural representations. Implicit neural representations learn a continuous mapping from local coordinates to the signal value such as intensity for images and videos, and occupancy value for 3D volumes. The learned models are then used for a myriad of tasks including image representations [Chen et al. 2021b], multi-view rendering [Mildenhall et al. 2020], and solving linear inverse problems [Sun et al. 2021]. Recent advances in the choice of coordinate representation [Tancik et al. 2020] and non-linearity [Sitzmann et al. 2020] have resulted in training processes that have high fitting accuracy. Salient works related to implicit representations include the NeRF representations [Mildenhall et al. 2020] and its many derivatives that seek to learn the 3D geometry from a set of multi-view images. Despite the interest and success of these implicit representation, current approaches often require millions of parameters. This culminates in a large memory footprint and training times, precluding representation of very high-dimensional signals.

Architectural changes for faster learning. Several interesting modifications have been proposed to increase training or inference speed. KiloNeRF [Reiser et al. 2021] replaced the large MLP with multiple small MLPs that fit only a small, disjoint part of the 3D space. This drastically speeds up the inference time (often by 60×), but has no effect on the training process itself. ACORN [Martel et al. 2021] utilized an adaptive coordinate decomposition to efficiently fit various signals. By utilizing a combination of integer programming and interpolation, ACORN reduced training time for fitting of images and 3D point clouds by one to two orders of magnitude compared to techniques like SIREN [Sitzmann et al. 2020] and convolutional occupancy network [Peng et al. 2020]. However, ACORN does not leverage cross-scale similarity of visual signals which often leads to long times to convergence for very large signals. Moreover, the adaptive optimized blocks calls for complex integer programming which can be prohibitively expensive.

Multi-scale representations. Visual signals are similar across scales, and this has been exploited for a wide variety of applications. In computer vision and image processing, wavelet transform and Laplacian pyramids are often used to efficiently perform tasks such as image registration [Thévenaz and Unser 2000], optical flow computation [Weber and Malik 1995], and feature extraction [Lowe 2004]. Multi-scale representations such as octrees [Chien and Agarwal 1986; Meagher 1982] and mip-mapping are used to speed up the rendering pipeline. This has also inspired neural mipmapping techniques [Kuznetsov et al. 2021] that utilize neural networks to represent texture at each scale. Multi-scale representations are also utilized for several linear inverse problems such as multi-scale dictionary learning for denoising [Sulam et al. 2014], compressive sensing [Park and Wakin 2009], and sparse approximation [Mairal

et al. 2007]. Some recent works have focused on a level-of-detail approach to neural representations [Takikawa et al. 2021] where the multiple scales are *jointly* learned. While efficient in rendering, the technique does not target extremely large meshes. MINER also results in an LOD representation, but the underlying approach is significantly different. MINER relies on a block-wise representation at each scale, which enables more compact representation with faster training times.

3 MINER

MINER leverages a block decomposition of signal along with a Laplacian pyramid-like representation. We now details the proposed signal model and the training process.

3.1 Signal model

Let \mathbf{x} be the coordinate and $I(\mathbf{x})$ be the target. We will assume that the coordinates lie in $[-1, 1]$. Let \mathcal{D}_j be the domain specific operator that downsamples the signal by j times, and \mathcal{U}_j be the domain-specific operator that upsamples the signal by j times. We will leverage J implicit representations, $I_j(\mathbf{x}) \approx N_j$ for $j \in [0, J-1]$, where N_j is the MLP at the j^{th} level of a Laplacian pyramid, a multiscale representation which separates the input signal into scales capturing unique spatial frequency bands. Two desirable properties of such a bandpass pyramid is that signals across scales are approximately orthogonal to one another [Do and Vetterli 2003], and are sparse. We find in our experiments that these properties help reduce training and inference times compared to a lowpass pyramid such as the Gaussian pyramid (see Fig. 3).

Letting R_j denote the MLP modeling the residual signal at scale j , our Laplacian pyramid representation may be written as:

$$I_{j-1}(\mathbf{x}) = \mathcal{D}_{j-1}(I(\mathbf{x})) \approx N_{j-1}(\mathbf{x}) \quad (1)$$

$$I_{j-2}(\mathbf{x}) = \mathcal{D}_{j-2}(I(\mathbf{x})) \approx R_{j-2}(\mathbf{x}) + \mathcal{U}_2(N_{j-1}(\mathbf{x}/2)) \quad (2)$$

$$\vdots$$

$$I(\mathbf{x}) \approx R_0(\mathbf{x}) + \mathcal{U}_2(N_1(\mathbf{x}/2)) \quad (3)$$

$$\approx N_0(\mathbf{x}) + \mathcal{U}_2(N_1(\mathbf{x}/2)) + \mathcal{U}_{2J-1}(N_{J-1}(\mathbf{x}/2^{J-1})), \quad (4)$$

where Equation (1) is the coarsest representation of the signal. At finer scales (as in Equation (2)), we write the signal to be approximated as a sum of the upsampled version of the previous scale and a residual term. This leads to a recursive multi-resolution representation that naturally shares information across scales.

We make two observations about the proposed multiscale representation:

- Signals at coarser resolutions are smaller, and therefore require smaller MLPs. These MLPs are faster for inference, which is beneficial for tasks such as mipmapping and LOD-based rendering.
- The parameters of the MLPs up to scale j only rely on the signal at scales $q = j, j+1, \dots, J-1$. This implies the MLPs can be trained *sequentially* from coarsest to finest scale. We will see next that this offers a dramatic reduction in training time without sacrificing quality.

3.1.1 Using multiple MLPs per scale. Equation (4) implies that obtaining a value at a spatial point \mathbf{x} requires evaluating a total of J

MLPs across scales. This is not beneficial compared to a single scale solution such as SIREN [Sitzmann et al. 2020]. Further, the residual signals at finer scales are often low-amplitude, a consequence of visual signals being composed of several smooth areas. To leverage this fact and make inference faster, we split the signal into equal sized blocks at each scale. We create an MLP for each block that requires significantly fewer parameters than a single full MLP at that scale. Moreover, blocks with small residual energy can be represented as a zero signal, and do not even need to be represented with an MLP.

We now combine the Laplacian representation with the multi-MLP approach stated above. Let $\tilde{\mathbf{x}}$ be a local coordinate at the finest scale in a block with coordinate (m, n) , where $m \in 1, 2, \dots, M$ is the number of vertical blocks, and $n \in 1, 2, \dots, N$ is the number of horizontal blocks. To evaluate the signal at \mathbf{x} we compute,

$$I(\mathbf{x}) = I\left(\tilde{\mathbf{x}} + \left\lfloor \frac{mH}{M}, \frac{nW}{N} \right\rfloor\right) = \mathcal{R}_0^{(m,n)}\left(\tilde{\mathbf{x}} + \left\lfloor \frac{mH}{M}, \frac{nW}{N} \right\rfloor\right) + \dots + \dots \mathcal{U}_2\left(\mathcal{N}_1^{(\lfloor m/2 \rfloor, \lfloor n/2 \rfloor)}\left(\tilde{\mathbf{x}} + \left\lfloor \frac{mH}{2M}, \frac{nW}{2N} \right\rfloor\right)\right), \quad (5)$$

where $\lfloor \cdot \rfloor$ is the floor operator, and $\mathcal{N}_j^{(m,n)}$ is the MLP for block at (m, n) and at scale j . With this formulation, we require evaluation of at most J small MLPs instead of large MLPs, thereby dramatically reducing inference time.

3.2 Training MINER

MINER requires estimation of parameters at each scale and each block. We now present an efficient *sequential* training procedure that starts at the coarsest scale and trains up to the finest scale.

Training at coarsest scale. The training process starts by fitting $I_{J-1}(\mathbf{x})$, the image at the coarsest scale. We estimate the parameters of each of the MLPs $\mathcal{N}_{J-1}^{(m,n)}$ by solving the objective function,

$$\min_{\mathcal{N}_{J-1}^{(m,n)}} \left\| I_{J-1}\left(\tilde{\mathbf{x}} + \left(\frac{mH}{2^{J-1}M}, \frac{nW}{2^{J-1}N}\right)\right) - \mathcal{N}_{J-1}^{(m,n)}(\tilde{\mathbf{x}}) \right\|^2. \quad (6)$$

Let $\hat{I}_{J-1}(\mathbf{x}_{J-1})$ be the estimate of the image at this stage.

Pruning at convergence. As the training proceeds, some MLPs, particularly for simpler blocks, will converge to a target mean squared error (MSE) earlier than others. We remove those MLPs that have finished training from the optimization process and continue with the others.

Training at finer scales. As with the coarsest scale, we continue to fit small MLPs to blocks at each finer scale. For example, for scale $J-2$, the target signal is given by

$$R_{J-2}(\mathbf{x}) = I_{J-2}(\mathbf{x}) - \mathcal{U}_2(\hat{I}_{J-1})(\mathbf{x}/2). \quad (7)$$

We leverage the fact that blocks within each scale occupy disjoint regions and can optimize each MLP independently of one another:

$$\min_{\mathcal{R}_{J-2}^{(m,n)}} \left\| R_{J-2}\left(\tilde{\mathbf{x}} + \left(\frac{mH}{2^{J-2}M}, \frac{nW}{2^{J-2}N}\right)\right) - \mathcal{R}_{J-2}^{(m,n)}(\tilde{\mathbf{x}}) \right\|^2. \quad (8)$$

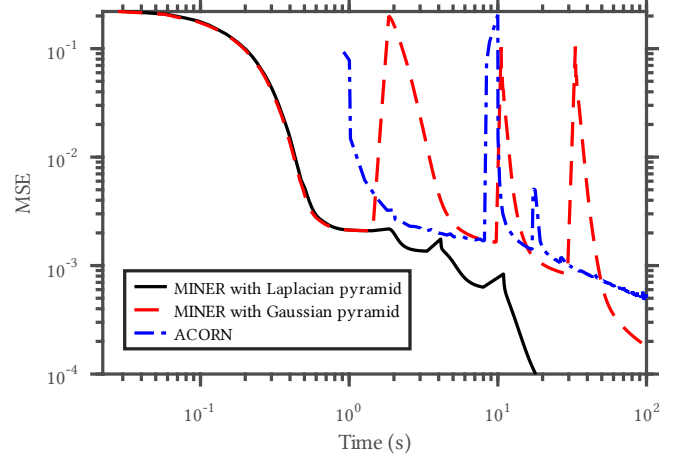


Fig. 3. **Laplacian pyramid enables faster convergence.** The plot above shows training error across time for a 2048×2048 image of Pluto. MINER when combined with a Laplacian pyramid offers a significantly faster convergence as the MLPs at finer scale capture orthogonal information compared to the coarser ones. This also results in very small jumps in training accuracy that is strongly prevalent when MINER is trained with a Gaussian pyramid, or ACORN.

Pruning before optimization. Nominally, the number of blocks and MLPs double along each dimension at finer scales. However, some blocks may already be adequately represented by the corresponding MLP at the coarser scale. In such a case, we do not assign an MLP to that block and set the estimate of the residue to all zeros. Depending on the frequency content in the image, this decision dramatically reduces the number of total MLP parameters, and thereby the overall training and inference times.

4 EXPERIMENTAL RESULTS

Baselines. For fitting to images and 3D volumes, we compared MINER against SIREN [Sitzmann et al. 2020], KiloNeRF [Reiser et al. 2021], and ACORN [Martel et al. 2021]. We also compared MINER Against convolutional occupancy networks [Peng et al. 2020] for 3D volumes. We used code from the respective authors and optimized the training parameters to ensure a fair comparison.

Training details. We implemented MINER with the PyTorch [Paszke et al. 2019] framework. Multiple MLPs were trained efficiently using the block matrix multiplication function (`torch.bmm`) and hence we required no complex coding outside stock pytorch implementations. All our models were trained on a system unit equipped with Intel Xeon 8260 running at 2.4Ghz, 128GB RAM, and NVIDIA GeForce RTX 2080 Ti with 12GB memory.

Fitting images. We split up RGB images into $32 \times 32 \times 3$ patches at all spatial scales. For each patch and at each scale, we trained a single MLP with four layers with sinusoidal activation function. We fixed the number of features to be 20 for each layer. We used the ADAM [Kingma and Ba 2015] optimizer with a learning rate of 5×10^{-4} and an exponential decay with $\gamma = 0.999$. At each scale, we trained either for 500 epochs, or until the change in loss function

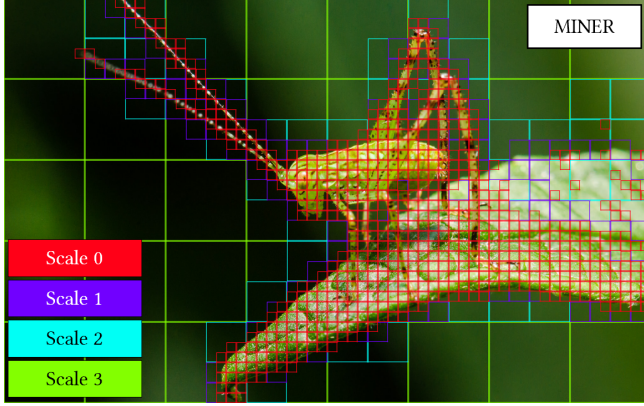


Fig. 4. **MINER adaptively selects window sizes.** MINER adaptively selects the appropriate scale for each local area resulting in patch sizes that are chosen according to texture variations within the window. The figure above shows a macro photograph of a grasshopper fit by MINER. Large parts of the image such as background have very smooth texture implying that they can be fit accurately at a coarser scale – which translates to large spatial size for low frequency areas. In contrast, area around the antennae are made of high spatial frequencies, which required fitting at finer scales.

was greater than 2×10^{-7} . We used an ℓ_2 loss function at all scales with no additional prior.

Figure 3 shows training error for a 4 megapixel (MP) image of Pluto across epochs for MINER by representing a Laplacian pyramid, a Gaussian pyramid, and ACORN. MINER converges rapidly to an error of 10^{-4} compared to other approaches. Moreover, the periodic and abrupt increase in error are more prevalent in Gaussian representation, and ACORN, which further hamper their performance, but not with Laplacian pyramid due to near-orthogonality of signal across scales. Results on other high resolution images (including 64 megapixel image of Pluto) along with analysis on effect of parameters such as number of scales and patch size is included in section 2.

Figure 4 shows an example of fitting a 2 megapixel image with active blocks at all scales for a macro photograph. Notice how the blocks are concentrated around the high frequency areas (such as the antennae of the grasshopper) as the scale increase from coarse to fine. MINER took a less than 10s to converge to 40dB fitting accuracy. In contrast, KiloNeRF took 6 minutes to converge and ACORN took 7 minutes to converge to 40dB with approximately equal number of parameters. Figure 5 shows a plot of PSNR as a function of time for various approaches. We also note that ACORN curve shows significant drop in accuracy as a result of re-computation of coordinate blocks. In contrast, the drop in accuracy for the MINER curve that arises due to scale change is significantly smaller than ACORN.

Figure 6 compares MINER, KiloNeRF, and ACORN in terms of time taken to achieve 36dB, and GPU memory for fitting 16MP image of Pluto. For all three cases, we varied the number of hidden features and fixed the number of layers to vary the number of parameters. MINER consistently achieves 36dB faster than competing methods and requires significantly smaller memory footprint, making it highly scalable for large-sized problems.

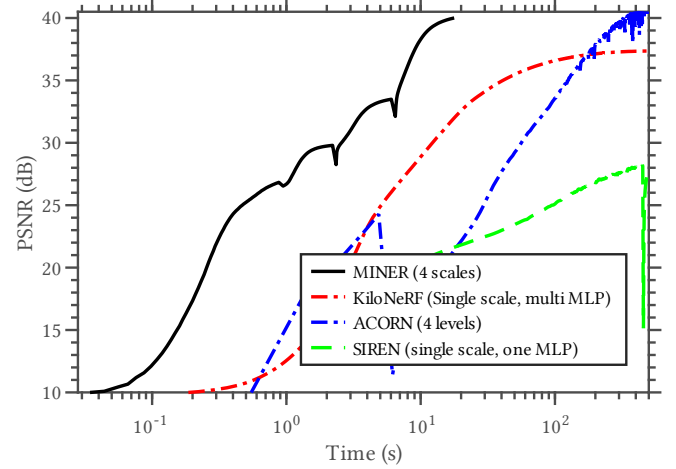


Fig. 5. **MINER converges 10× faster than state-of-the-art approaches.** The plot shows PSNR as a function of time for various approaches for the image shown in Fig. 4. MINER achieves higher accuracy at all times, and converges significantly faster than competing approaches. Moreover, the drop in accuracy when changing from coarse to fine scale is less severe for MINER compared to when ACORN re-estimates coordinate decomposition.

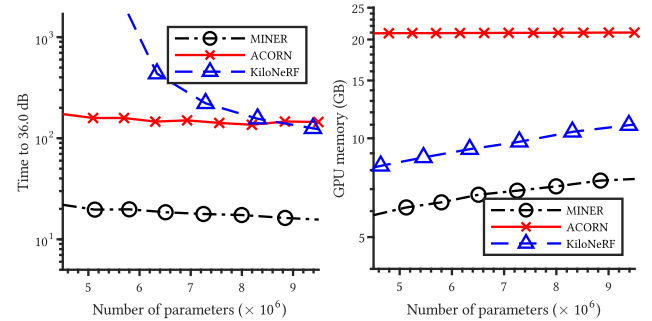


Fig. 6. **MINER requires shorter training time and memory footprint.** The plot shows the time taken to achieve 36 dB and the GPU memory utilization to fit a 16MP image (Pluto) with ACORN and MINER for varying number of parameters. MINER is an order of magnitude faster than ACORN and requires less than one third of the GPU memory as ACORN – implying MINER is well-suited to train very large models.

MINER scales up gracefully for extremely large signals. We trained ACORN on a gigapixel image shown in Fig. 7 over 7 scales. We set the number of features per each block to be 9, and used a patch size of 32×32 . MINER converged to a PSNR of 38.6dB in 2.6h and required a total of 188 million parameters. In contrast, ACORN converged to the same accuracy in 36h and required a total of 167 million parameters. Note that although MINER requires more parameters than ACORN, the training time is shorter. Since MINER leverages numerous small MLPs, the backpropagation step requires significantly fewer computations.

Fitting 3D point clouds. Inspired by Convolutional occupancy networks [Peng et al. 2020], we utilized signed density function where the value was 1 inside the mesh and 0 outside. We sampled a total



Fig. 7. **Fitting gigapixel images.** The figure shows the results on fitting a gigapixel image ($20,480 \times 56,420$) with MINER and ACORN. MINER required 188 million parameters and converged to 38.6dB in 2.6 hours. In contrast, ACORN required 167 million parameters and converged to 32.6dB in 48 hours.

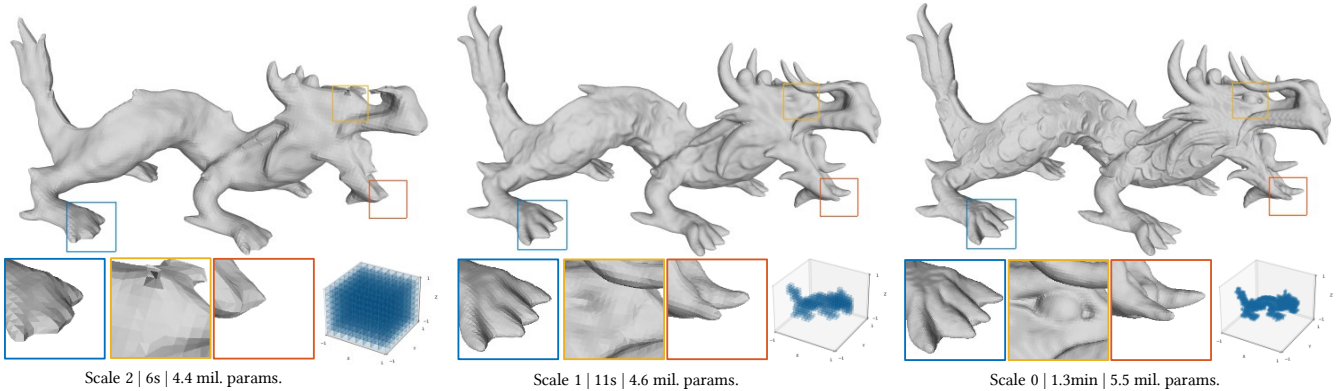


Fig. 8. **Active blocks reduce with increasing scale.** The figure shows MINER results at the end of training at each scale (left column) and the active blocks at each scale (right column). As the iterations progress, only the blocks on the surface of the object remain, which leads to a dramatic reduction in non-zero blocks, and hence the total number of parameters.

of one billion points, resulting in a $1024 \times 1024 \times 1024$ occupancy volume. We then optimized MINER over four scales for a maximum of 2000 iterations at each scale. We experimented with logistic loss and MSE and found the MSE resulting in significantly faster convergence. The learning rate was set to 10^{-3} . We set the number

of features to 22 and the number of hidden layers to 2 for MLP for each block at all scales. We then constructed mesh from the resultant occupancy volumes using marching cubes [Lorensen and Cline 1987]. We compared our results against ACORN, and convolutional occupancy networks for accuracy and timing comparison,

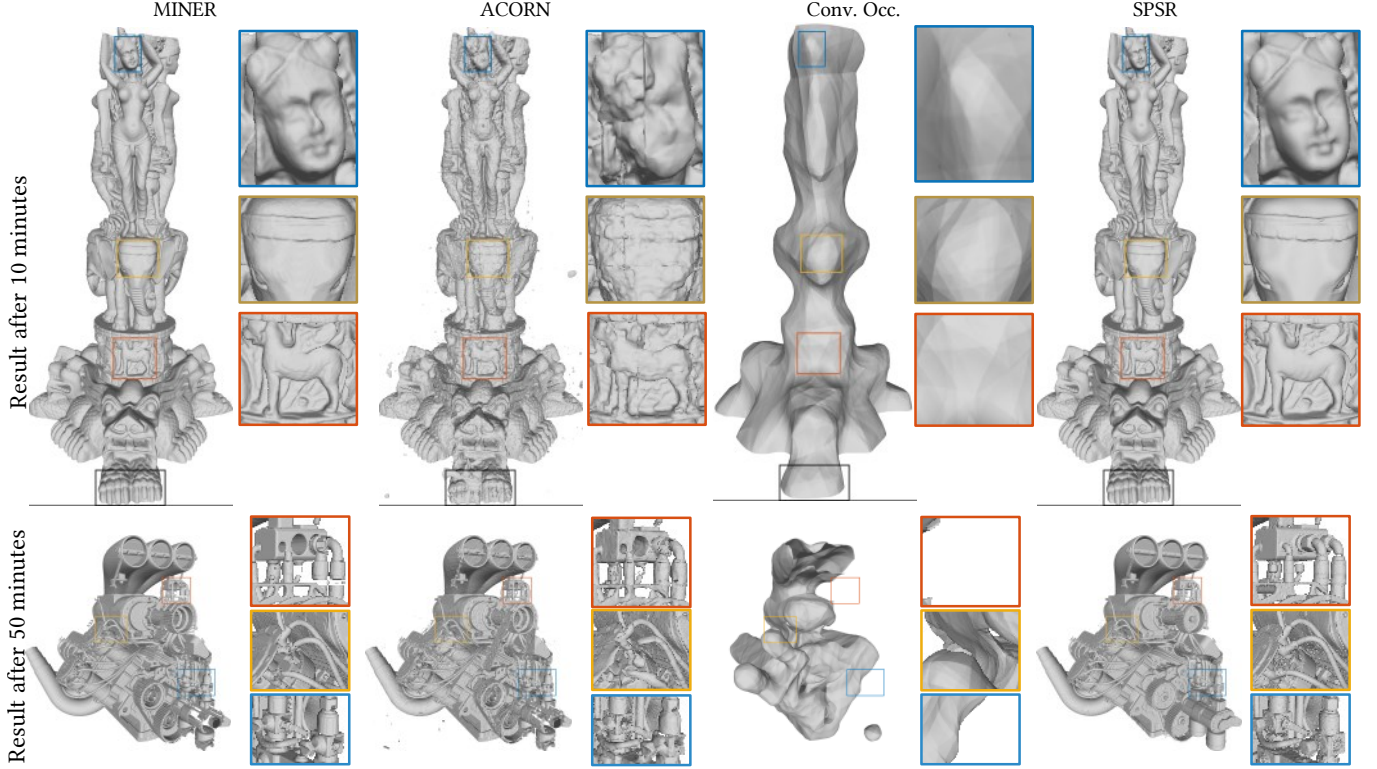


Fig. 9. **Comparisons against state-of-the-art for 3D volume fitting.** The figure compares 3D occupancy fitting for a **fixed duration** with MINER, ACORN, Convolutional occupancy [Peng et al. 2020], and screening poisson reconstruction [Kazhdan and Hoppe 2013]. The number of parameters of MINER was chosen automatically according to model complexity. MINER achieves high accuracy in a very short duration for arbitrarily complex shapes, which is not possible with prior works, even though some models such as the engine (second row) require significantly larger number of parameters.

and screened poisson reconstruction (SPSR) [Kazhdan and Hoppe 2013] for comparing quality of reconstruction. For SPSR, which takes in point clouds, we sampled 5 million points from the object’s surface as input.

Figure 1 shows the active blocks and reconstructed mesh at each scale. MINER converges in less than 25 minutes to an Intersection over Union (IoU) of 0.999. In the same time, ACORN achieved an IoU of 0.97 with worse results than MINER. ACORN took greater than 7 hours to converge to an IoU of 0.999, clearly demonstrating the advantages of MINER for 3D volumes. We also note that MINER required less than a third as the number of parameters as ACORN – this is a direct consequence of using block-based representation – most blocks outside the mesh and inside the mesh converge rapidly within the first few scales, requiring far fewer representations than a single scale representation. An example of active blocks at each scale is shown in Fig. 8. As iterations progress, the number of active blocks after pruning reduce, which in turn results in more compact representation, and fewer parameters.

Figure 9 visualizes the meshes fit with various reconstruction approaches for a fixed duration. The time for each experiment was chosen to be when MINER Achieved an IoU of 0.999. MINER has superior reconstruction quality compared to ACORN and convolutional occupancy networks [Peng et al. 2020], and comparable

performance to SPSR. We do note that the quality of reconstruction specifically for the engine model is superior to SPSR. Since the engine model has a large number of sharp edges, SPSR tends to oversmooth the result. Since MINER combined with marching cubes relied only on local information for reconstruction, the resultant mesh was more accurate.

5 CONCLUSIONS

We have proposed a novel multi-scale neural representation that trains faster, requires same or fewer parameters, and has lower memory footprint than state-of-the-art approaches. We demonstrated that the advantages of a Laplacian pyramid naturally extend to MINER. We showed that leveraging self-similarity across scales is beneficial in reducing training time drastically while not affecting the training accuracy. MINER naturally lends itself to rendering where level-of-detail is of importance including representation and mipmapping for texture mapping. Future directions will focus on combining MINER with multi-view synthesis to achieve extremely fast fitting and visualization pipelines that will open avenues for training highly complex geometric shapes.

6 ACKNOWLEDGMENTS

This work was supported by NSF grants CCF-1911094, IIS-1838177, and IIS-1730574; ONR grants N00014-18-12571, N00014-20-1-2534, and MURI N00014-20-1-2787; AFOSR grant FA9550-22-1-0060; and a Vannevar Bush Faculty Fellowship, ONR grant N00014-18-1-2047.

7 APPENDIX 1: ALGORITHM DETAILS

Algorithm 1 shows the overall MINER flow with initialization, pruning, and parameter update. The function DOWNSAMPLE implements a domain-specific downsampling operator. For images it is,

$$\mathcal{D}_j(I) = I_j(\mathbf{x}) = \int_0^{2^j/H} \int_0^{2^j/W} I(2^j \mathbf{x} + d\mathbf{x}) dx dy. \quad (9)$$

For three-dimensional signals such as videos $(I(x, y, t))$ and 3D occupancy volumes $(I(x, y, z))$ we have,

$$\mathcal{D}_j(I) = I_j(\mathbf{x}) = \int_0^{2^j/H} \int_0^{2^j/W} \int_0^{2^j/T} I(2^j \mathbf{x} + d\mathbf{x}) dx dy dz. \quad (10)$$

8 APPENDIX 2: EXPERIMENTAL RESULTS

Baselines. We compare MINER against three competing baselines for 2D images, and three for 3D volumes.

- (1) SIREN [Sitzmann et al. 2020] fits a single large MLP at a single scale and utilizes a sinusoidal activation function for accelerated training. We varied the number of hidden units for each experiment to ensure that the number of parameters matched that of MINER.
- (2) KiloNeRF [Reiser et al. 2021] fits multiple small MLPs at a single scale instead of a single large MLP. The number of hidden units for each MLP was chosen to be the same as that for MINER.
- (3) ACORN [Martel et al. 2021] fits a single large MLP at a single scale with adaptive coordinate decomposition.
- (4) Convolutional occupancy network [Peng et al. 2020] utilizes convolutions to capture local correlations. We used this only for 3D volume comparisons.

We used code from the respective authors and optimized the training parameters to ensure a fair comparison.

Fitting images. Figure 10 shows fitting result for 64 megapixel Pluto image across training iterations. The times correspond to the instances when MINER converged at a given scale. MINER maintains high quality reconstruction at all instances due to the multiscale training scheme and rapidly converges to a PSNR of 40dB within 50 seconds. In contrast, ACORN achieves qualitatively good results after 10s and achieves a PSNR of 30.8 dB after 50s, and KiloNeRF achieves a qualitatively good result only after 50s. SIREN Results are not shown in the plot as the first result was produced after 4 minutes. Figure 11 shows the gigapixel image from the main paper fit over 7 scales along with more insets.

Fitting 3D point clouds. Figure 12 visualizes the meshes fit with various reconstruction approaches for a fixed duration. MINER has superior reconstruction quality compared to ACORN and convolutional occupancy networks [Peng et al. 2020], and comparable performance to SPSR. We do note that the quality of reconstruction specifically for the engine model is superior to SPSR. Since the engine model has a large number of sharp edges, SPSR tends to

Algorithm 1 MINER algorithm.

Require: $I(\mathbf{x})$, number of scales J , block size b , number of features per layer N_{feat} , number of layers N_{layers}

for $j = J - 1, J - 2, \dots, 0$ **do** ▷ Loop over spatial scales

if j is $J - 1$ **then**

$R_j(\mathbf{x}_j) \leftarrow \text{DOWNSAMPLE}(I(\mathbf{x}), 1/2^{J-1})$

end if

$Q_j \leftarrow \frac{HW}{2^j b^2}$ ▷ Number of blocks

$A_j \leftarrow \{1, 2, \dots, Q_j\}$ ▷ Active set

for $q = 1, 2, \dots, Q_j$ **do** ▷ Loop over blocks

if $\|R_j(\mathbf{x}_j^q)\| \leq \tau_j$ **then**

$A_j \leftarrow A_j \setminus q$ ▷ Remove converged blocks

else

$\mathcal{N}_j^q \leftarrow \text{MLP}(N_{\text{feat}}, N_{\text{layers}})$ ▷ MLPs for each block

if $j < J - 2$ **then**

$k_q \leftarrow \text{PARENT}(q)$

$\theta_j^q \leftarrow \theta_j^{k_q} / 2$ ▷ Weight sharing for images

$\theta_j^q \leftarrow \theta_j^{k_q} / \sqrt{8}$ ▷ Weight sharing for 3D volumes

end if

end if

end for

for $i = 1, 2, \dots, N_{\text{iter}}$ **do**

for q in A_j **do**

$\hat{I}(\mathbf{x}_j^q) \leftarrow \mathcal{N}_j^q(\mathbf{x}_j^q)$ ▷ Compute MLP output

$\epsilon_j^q \leftarrow \|\hat{I}(\mathbf{x}_j^q) - I(\mathbf{x}_j^q)\|^2$ ▷ Compute MSE loss

 Backpropagate ϵ_j^q to update θ_j^q

if $\epsilon_j^q \leq \tau_j$ **then**

$A_j \leftarrow A_j \setminus q$ ▷ Prune converged blocks

end if

end for

end for

oversmooth the result. Since MINER combined with marching cubes relied only on local information for reconstruction, the resultant mesh was more accurate.

8.1 Analysis of parameter space

The training time of MINER is affected by number of scales, size of each patch, stopping criteria when switching to a finer scale, and parameters of each MLP including number of layers, number of features per layer and the type of non-linearity. We now provide a thorough analysis of the parameters.

Performance with varying patch size. The optimal patch size is highly dependent on the signal itself. To understand the empirical relationship, we fit three types of images with low, medium, and high texture content using MINER to achieve 40dB accuracy. In each case, we varied the patch size from 8 pixels to 64 pixels. We proportionally increased the number of features per layer for each patch to keep the total number of parameters approximately the same. Figure 13 shows the plot of time taken to achieve 40 dB as a function of patch size for the three images. We notice that the

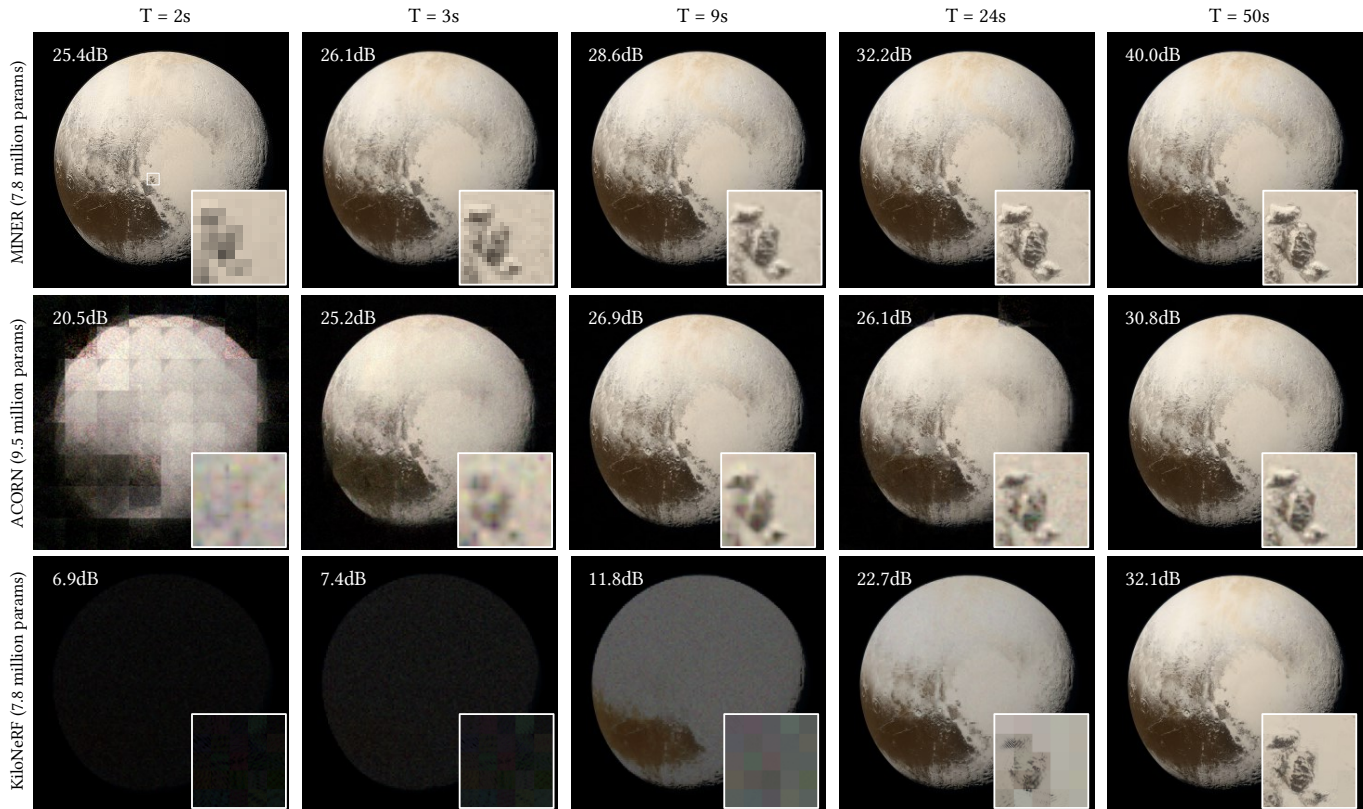


Fig. 10. **Image fit over time.** The figure compares fitting of the 16 megapixel pluto image at various times during the training process. A distinct advantage of MINER is that the signal is similar to the final output (albeit downsampled) from the starting itself which enables an easy visual debug of the fitting process.

optimal patch size for least training time increases with reducing texture content – which can be used as a guideline when choosing the appropriate patch size.

Performance with number of scales. Figure 14 shows the time taken to achieve 40dB on the pluto image with varying number of spatial scales. We note that increasing the number of scales is beneficial up to four scales, but the performance deteriorates after that.

REFERENCES

- Edward H Adelson, Charles H Anderson, James R Bergen, Peter J Burt, and Joan M Ogden. 1984. Pyramid methods in image processing. *RCA Engineer* 29, 6 (1984), 33–41.
- Hao Chen, Bo He, Hanyu Wang, Yixuan Ren, Ser Nam Lim, and Abhinav Shrivastava. 2021a. Nerv: Neural representations for videos. *Adv. Neural Info. Processing Systems* (2021).
- Yinbo Chen, Sifei Liu, and Xiaolong Wang. 2021b. Learning continuous image representation with local implicit image function. In *IEEE Comp. Vision and Pattern Recognition (CVPR)*.
- Chiun-Hong Chien and Jake K Aggarwal. 1986. Volume/surface octrees for the representation of three-dimensional objects. *Computer Vision, Graphics, and Image Processing* 36, 1 (1986), 100–113.
- Minh N Do and Martin Vetterli. 2003. Framing pyramids. *IEEE Trans. Signal Processing* 51, 9 (2003), 2329–2342.
- Michael Kazhdan and Hugues Hoppe. 2013. Screened poisson surface reconstruction. *ACM Trans. Graphics* 32, 3 (2013), 1–13.
- Diederik P. Kingma and Jimmy Ba. 2015. Adam: A Method for Stochastic Optimization. In *Intl. Conf. Learning Representations*.
- Alexandr Kuznetsov, Krishna Mullia, Zexiang Xu, Miloš Hašan, and Ravi Ramamoorthi. 2021. NeuMIP: Multi-resolution neural materials. *ACM Trans. Graphics* 40, 4 (2021), 1–13.
- William E Lorensen and Harvey E Cline. 1987. Marching cubes: A high resolution 3D surface construction algorithm. *ACM SIGGRAPH* 21, 4 (1987), 163–169.
- David G Lowe. 2004. Distinctive image features from scale-invariant keypoints. *Intl. J. Computer Vision* 60, 2 (2004), 91–110.
- Julien Mairal, Guillermo Sapiro, and Michael Elad. 2007. Multiscale sparse image representation with learned dictionaries. In *IEEE Intl. Conf. Image Processing (ICIP)*, Vol. 3. III–105.
- Julien NP Martel, David B Lindell, Connor Z Lin, Eric R Chan, Marco Monteiro, and Gordon Wetzstein. 2021. ACORN: Adaptive Coordinate Networks for Neural Scene Representation. *arXiv preprint arXiv:2105.02788* (2021).
- Donald Meagher. 1982. Geometric modeling using octree encoding. *Computer Graphics and Image Processing* 19, 2 (1982), 129–147.
- Ben Mildenhall, Pratul P Srinivasan, Matthew Tancik, Jonathan T Barron, Ravi Ramamoorthi, and Ren Ng. 2020. Nerf: Representing scenes as neural radiance fields for view synthesis. In *IEEE European Conf. Computer Vision (ECCV)*.
- Jae Young Park and Michael B Wakin. 2009. A multiscale framework for compressive sensing of video. In *Picture Coding Symposium*.
- Adam Paszke, Sam Gross, Francisco Massa, Adam Lerer, James Bradbury, Gregory Chanan, Trevor Killeen, Zeming Lin, Natalia Gimelshein, Luca Antiga, Alban Desmaison, Andreas Kopf, Edward Yang, Zachary DeVito, Martin Raison, Alykhan Tejani, Sasank Chilamkurthy, Benoit Steiner, Lu Fang, Junjie Bai, and Soumith Chintala. 2019. PyTorch: An Imperative Style, High-Performance Deep Learning Library. In *Adv. Neural Info. Processing Systems*.
- Songyou Peng, Michael Niemeyer, Lars Mescheder, Marc Pollefeys, and Andreas Geiger. 2020. Convolutional occupancy networks. In *IEEE European Conf. Computer Vision (ECCV)*.
- Christian Reiser, Songyou Peng, Yiyi Liao, and Andreas Geiger. 2021. KiloNeRF: Speeding up Neural Radiance Fields with Thousands of Tiny MLPs. *arXiv preprint arXiv:2103.13744* (2021).
- Jerome M Shapiro. 2009. Embedded image coding using zerotrees of wavelet coefficients. In *Fundamental Papers in Wavelet Theory*. 861–878.



Fig. 11. **Fitting gigapixel images.** The figure shows the results on fitting a gigapixel image ($20,480 \times 56,420$) with MINER and ACORN. MINER required 188 million parameters and converged to 38.6dB in 2.6 hours. In contrast, ACORN required 167 million parameters and converged to 32.6dB in 48 hours.

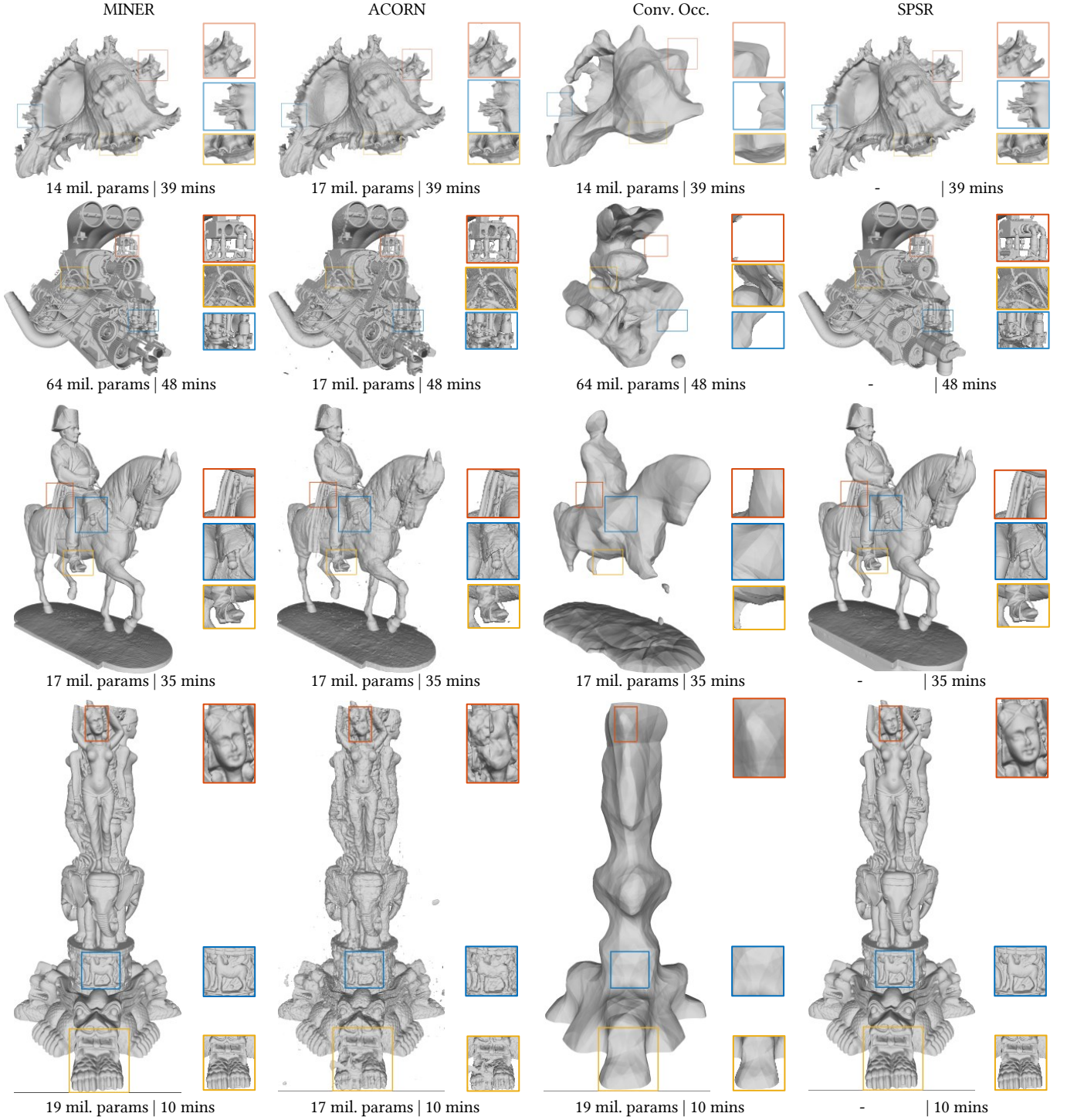


Fig. 12. **Comparisons against state-of-the-art for 3D volume fitting.** The figure compares 3D occupancy fitting for a **fixed duration** with MINER, ACORN, Convolutional occupancy [Peng et al. 2020], and screening poisson reconstruction [Kazhdan and Hoppe 2013]. The number of parameters of MINER was chosen automatically according to model complexity. MINER achieves high accuracy in a very short duration for arbitrarily complex shapes, which is not possible with prior works, even though some models such as the engine (second row) require significantly larger number of parameters.

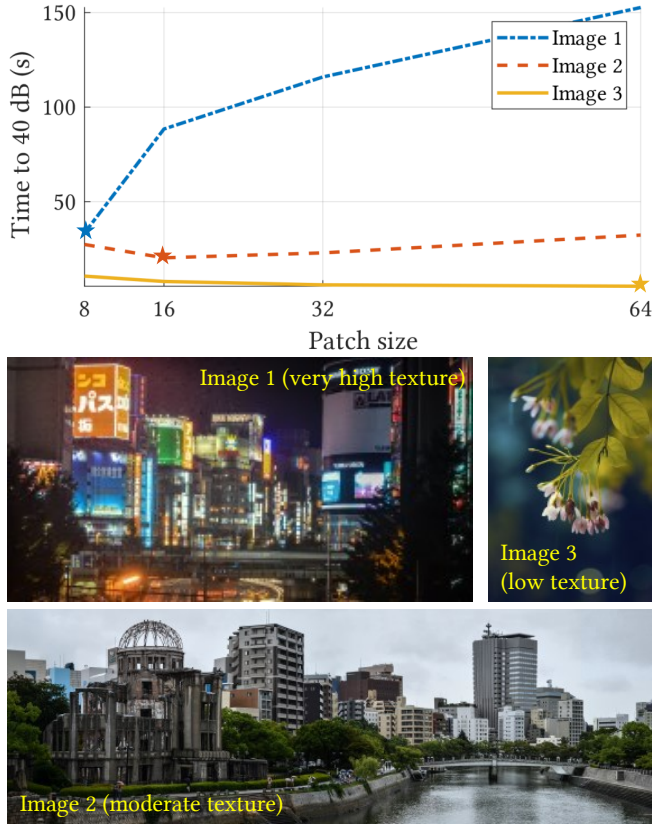


Fig. 13. **Effect of patch size.** The plot shows the time taken to achieve 40 dB for three different images. We notice that the optimal patch size is highly dependent on the image. For images with high texture content (image 1), a smaller patch size of 8 pixels is optimal. For medium texture with large flat areas (image 2), a medium patch size of 32 pixels is optimal. For images such as macro photography (image 3) which has strong low frequency content, larger patch size of 64 is optimal.

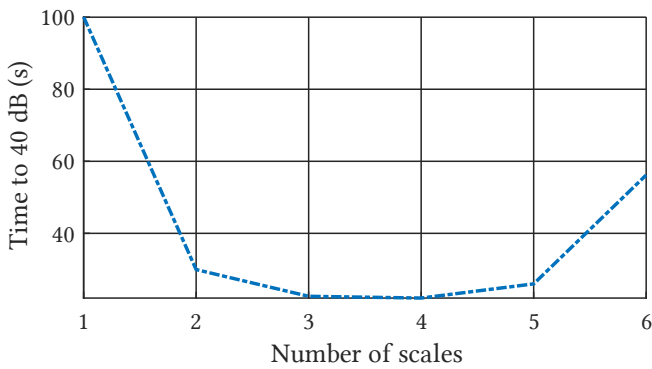


Fig. 14. **Effect of number of scales.** The plot shows the time taken to fit a 16MP image (Pluto) with MINER with varying number of spatial scales. Performance increases up to 4 scales but then degrades

Adv. Neural Info. Processing Systems (2020).

- Pratul P Srinivasan, Boyang Deng, Xiuming Zhang, Matthew Tancik, Ben Mildenhall, and Jonathan T Barron. 2021. Nerv: Neural reflectance and visibility fields for relighting and view synthesis. In *IEEE Comp. Vision and Pattern Recognition (CVPR)*.
- Jeremias Sulam, Boaz Ophir, and Michael Elad. 2014. Image denoising through multi-scale learnt dictionaries. In *IEEE Intl. Conf. Image Processing (ICIP)*.
- Yu Sun, Jiaming Liu, Mingyang Xie, Brendt Wohlberg, and Ulugbek S Kamilov. 2021. Coil: Coordinate-based internal learning for imaging inverse problems. *arXiv preprint arXiv:2102.05181* (2021).
- Towaki Takikawa, Joey Litalien, Kangxue Yin, Karsten Kreis, Charles Loop, Derek Nowrouzezahrai, Alec Jacobson, Morgan McGuire, and Sanja Fidler. 2021. Neural geometric level of detail: Real-time rendering with implicit 3D shapes. In *IEEE Comp. Vision and Pattern Recognition (CVPR)*.
- Matthew Tancik, Pratul P. Srinivasan, Ben Mildenhall, Sara Fridovich-Keil, Nithin Raghavan, Utkarsh Singhal, Ravi Ramamoorthi, Jonathan T. Barron, and Ren Ng. 2020. Fourier Features Let Networks Learn High Frequency Functions in Low Dimensional Domains. *Adv. Neural Info. Processing Systems* (2020).
- Philippe Thévenaz and Michael Unser. 2000. Optimization of mutual information for multiresolution image registration. *IEEE Trans. Image Processing* 9, 12 (2000), 2083–2099.
- Joseph Weber and Jitendra Malik. 1995. Robust computation of optical flow in a multi-scale differential framework. *Intl. J. Computer Vision* 14, 1 (1995), 67–81.
- Alex Yu, Ruilong Li, Matthew Tancik, Hao Li, Ren Ng, and Angjoo Kanazawa. 2021. Plenotrees for real-time rendering of neural radiance fields. *arXiv preprint arXiv:2103.14024* (2021).

Vincent Sitzmann, Julien Martel, Alexander Bergman, David Lindell, and Gordon Wetzstein. 2020. Implicit neural representations with periodic activation functions.